Molecular dynamics simulation of diffusion of gases in a carbon-nanotube–polymer composite

Seong Y. Lim, Muhammad Sahimi,* Theodore T. Tsotsis, and Nayong Kim
Mork Family Department of Chemical Engineering & Materials Science, University of Southern California, Los Angeles, California 90089-1211, USA

(Received 28 October 2006; revised manuscript received 23 April 2007; published 31 July 2007)

Extensive molecular dynamics (MD) simulations were carried out to compute the solubilities and self-diffusivities of CO_2 and CH_4 in amorphous polyetherimide (PEI) and mixed-matrix PEI generated by inserting single-walled carbon nanotubes into the polymer. Atomistic models of PEI and its composites were generated using energy minimizations, MD simulations, and the polymer-consistent force field. Two types of polymer composite were generated by inserting (7,0) and (12,0) zigzag carbon nanotubes into the PEI structure. The morphologies of PEI and its composites were characterized by their densities, radial distribution functions, and the accessible free volumes, which were computed with probe molecules of different sizes. The distributions of the cavity volumes were computed using the Voronoi tessellation method. The computed self-diffusivities of the gases in the polymer composites are much larger than those in pure PEI. We find, however, that the increase is not due to diffusion of the gases *through* the nanotubes which have smooth energy surfaces and, therefore, provide fast transport paths. Instead, the MD simulations indicate a squeezing effect of the nanotubes on the polymer matrix that changes the composite polymers' free-volume distributions and makes them more sharply peaked. The presence of nanotubes also creates several cavities with large volumes that give rise to larger diffusivities in the polymer composites. This effect is due to the repulsive interactions between the polymer and the nanotubes. The solubilities of the gases in the polymer composites are also larger than those in pure PEI, hence indicating larger gas permeabilities for mixed-matrix PEI than PEI itself.

DOI: 10.1103/PhysRevE.76.011810 PACS number(s): 61.25.Hq, 02.70.Ns, 61.82.Pv, 81.07.De

I. INTRODUCTION

Nanoporous media constitute an important class of materials with a wide variety of applications. They include catalysts, membranes, adsorbents, and thin flims that are used not only in surface coating, but also as low-dielectric-constant materials, sensors, and insulators. In particular, membranes have been advocated for many years as a promising tool for the separation and purification of fluids [1–3], while biological membranes are also of immense importance to a variety of biological activities and functions. For example, separation by membranes of oxygen from air, enrichment of methane in the gas mixtures that landfills produce, and separation of H_2 and CO_2 from coal gasification processes have attracted considerable attention. In addition, an important impedement to the use of fuel cells has been the production of hydrogen with high degree of purity, which certain nanoporous membranes may be able to provide by separating H_2 from various gas mixtures.

Among many nanoporous membranes that have been prepared and advocated for various applications, carbon-molecular-sieve membranes (CMSMs), which are prepared by carbonization of a variety of polymeric precursors, have recently been studied as a promising alternative to both inorganic and polymeric membranes [4–8]. In particular, we have been using polyetherimide (PEI)—a high-temperature, glassy, amorphous polymer [8]—as the polymeric precursor in the preparation of CMSMs. The average pore size of CMSMs is typically less than 5 Å, because of which the molecular interactions between the gases that pass through the membranes' nanopores are important and cannot be ignored. Therefore, accurate studies of such nanoporous materials and sorption and transport of gases and liquids in them require detailed molecular modeling [9,10]. Over the past few years, we have been developing [11–13] atomistic models of CMSMs and of sorption and transport of low-molecular-weight gasess in them, using molecular dynamics (MD) simulations. Our models and studies have provided not only estimates of the macroscopic properties of interest, such as the effective diffusivity and solubility of various gases, but also detailed information on the mechanisms of transport processes in such materials. Since we have been using PEI as a polymeric precursor for the preparation of CMSMs [7,14], one goal of our study, in addition to being important and interesting on its own, has been gaining better understanding of the similarities and differences between transport and sorption in PEI—the precursor material—and CMSMs—the final nanoporous material made from the precursor.

Recent experiments indicated [14] that mixed-matrix membranes, composed of polyimide and CMSMs pyrolyzed from polyimide, exhibit much improved permeance and selectivity for the separation of various gas mixtures, such as CO_2/CH_4. At the same time, recent atomistic simulations of gases in single-walled carbon nanotubes [15,16] indicated very high gas permeances, rates of transport, and excellent separation properties. The purpose of the present paper is to report the preliminary results of a study for investigating the possibility of improving the performance of a polymeric membrane by inserting carbon nanotubes in its matrix. Using MD simulations, we study diffusion and solubility of CO_2 and CH_4 in PEI and in its composites, which we generate by inserting carbon nanotubes in PEI. Such a study is important not only on its own, as it explores the possibility of developing better polymeric membranes and composites, but can

*Corresponding author. moe@iran.usc.edu

also provide insight into improving the performance of CMSMs for which PEI is a precusor. Our study has been made possible by recent advances in computing and molecular simulation techniques that enable us to construct models of glassy amorphous polymers, such as PEI, with accurate interatomic potentials.

Only a relatively small number of studies has been devoted in the past to molecular modeling of diffusion (and sorption) in polymers, most of which have dealt with flexible polymeric chains composed of repeating units with a relatively simple structure, such as poly(dimethylsiloxane) (PDMS), poly(isobutylene), polyethylene (PE), and polypropylene [17–23]. Moreover, very few studies have focused on polymers that consist of stiff chains [24–26], as well as membrane materials, such as polyelectrolytes [27,28]. Mooney and MacElroy [28] studied, for example, diffusion of small molecules in semicrystalline aromatic polymers. There have been only a few papers using MD simulations to study the transport mechanism(s) in polymeric materials. For example, Tamai *et al.* [17] and Fritz and Hofmann [18] utilized MD simulations to study the diffusion and sorption of methane, water, and ethanol in PDMS and PE using a united-atom model in the bulk region, while Muller-Plathe [19] carried out MD simulation of diffusion of water in poly(vinyl alcohol), used as packaging materials. Very few studies have focused on the transport of small molecules through glassy polymers [28], calculating both the molecules' solubility and diffusivity. Generally speaking, while good qualitative agreement between simulation and experimental values of the diffusion coefficients and the solubilities has been obtained, only a few models have produced quantitative agreement with the experimental data. While tuning the parameters of the force field that represents the polymers improves the agreement between the computed and measured values, it has been shown that the size of the simulation cell itself [23] and the method of polymer generation [22] significantly affect the calculated molecular solubility in a polymer glass. The only work that we are aware of that investigates the properties of nanotube-polymer composites is that of Wei *et al.* [29] who used MD simulations to study the thermal expantion and transport characteristics of carbon nanotube-polyethylene composites. In addition, MD simulations were very recently utilized by Han and Elliot [30] to compute the elastic properties of polymer-canbon nanotube composites.

The rest of this paper is organized as follows. In Sec. II we present the details of the molecular modeling, including the atomistic models of PEI, its composites, MD simulation of gas diffusion in the materials, and computation of the free-volume distributions and the gases' solubilities. Section III contains the results of the study and their implications, while Sec. IV presents an in-depth discussion of the results. The last section summarizes the paper.

II. MOLECULAR MODELING AND SIMULATION

The MD simulations consist of two steps. First, we generate molecular models of PEI and also a mixed-matrix polymer (MMP) composite, consisting of PEI and carbon nanotubes, by the methods described below and compute the free-volume distributions and the solubilities. The next step is carrying out equilibrium MD simulations of the diffusion of CO_2 and CH_4 in PEI and MMP composites. In what follows, we describe the details of the computational techniques employed in our studies.

A. Generation of the polymer and its mixed-matrix composites

The PEI microstructure was generated using a modified version [31,32] of the self-avoiding walk (SAW) method of Theodorou and Suter [33]. Polymer generation starts by inserting three atoms in the backbone of the polymer, connected together by the bonds, in a cubic unit cell in a random orientation. The length of the backbone chain is then increased stepwise by adding one atom at a time to the growing polymer chain, using the modified SAW method. During the growth of the polymer, the allowed rotational states of successive bonds between adjacent atoms are determined from the probability distribution functions that are governed by energy considerations. The probability that a bond assumes a given orientation relative to an adjacent bond depends on the rotational state of the adjacent bond. Therefore, although an atom can be added to the growing polymer in a number of different orientations, only the particular orientation that results in the smallest increase in the potential energy of the polymer has the highest probability of forming. In this way polymers of a given length are constructed. The PEI structure was constructed using 40 repeating units, and a single polymer chain was inserted into the simulation cell in order to eliminate chain-end effects.

We used single-walled carbon nanotubes (SWCNTs) in order to generate nanotube–PEI-polymer composites. Two types of composite were generated using open-ended zigzag (7,0) and (12,0) nanotubes. (Use of other types of carbon nanotubes is currently being studied.) We refer to the two types of polymer composites as MMP7 and MMP12, respectively. The length of both nanotubes was about 14.4 Å, whereas their open-end diameters were 7 and 10.5 Å, respectively. In each case three nanotubes were inserted at randomly selected positions within the polymer matrix (without allowing overlap with the polymer's atoms) and their dangling ends were saturated with hydrogen atoms. Their final locations within the polymer were determined using energy minimization and MD simulations (see below). The weight fractions of the (7,0) and (12,0) nanotubes in the composites were 0.13 and 0.22, respectively. Figure 1 presents the structure of a repeating unit of PEI, together with that of the (7,0) nanotube. Minimum-image periodic boundary conditions were imposed on the cubic simulation cell in order to eliminate the boundary effects. The entire procedure for generating the structures of the materials and computing the various properties of interest was as follows.

In the case of pure PEI [13], the initial packing density in the simulation cell was set at 0.1 g/cm^3 (using a large simulation cell). The energy of the system was then minimized using conjugate-gradient algorithms [9]. The resulting structure was then compressed using MD simulation in a (*NPT*) ensemble under a pressure of 0.6 GPa for 10 ps in order to increase the polymer density to be as close to the experimen-

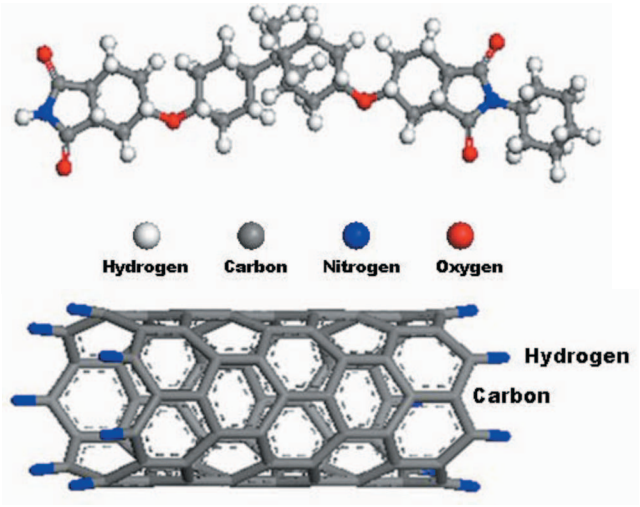

FIG. 1. (Color online) Repeating units of the PEI (top) structure and the zigzag (7,0) carbon nanotube (bottom).

tal value of 1.27 g/cm^3 as possible. Energy minimization and short-duration MD simulations in the (*NVT*) ensemble at 1000 K were then followed in order to further relax the material. Then, MD simulations were carried out in the (*NPT*) ensemble for several ns at 1 atm and 300 K. The gases' solubility and the free-volume distribution of the polymer were then computed. To compute the effective self-diffusivities of CO_2 and CH_4 in the PEI structure we followed the same procedure as above, except that, after generating the initial PEI structure by the SAW method, we inserted the gas molecules in the simulation cell (without allowing overlaps of the gases with the atoms of the PEI structure) and followed the energy-minimization–MD simulation procedure. We estimated the diffusivities by using both the (*NPT*) and (*NVT*) ensembles and, as discussed below, discovered some differences between the results obtained with the two ensembles.

In the case of MM PEI, after generating the polymer at low density, we inserted the SWCNTs at randomly selected points within the simulation cell, disallowing overlap with the atoms of the PEI structure. The same energy minimization, compression, and further relaxation steps as above were then followed. The gases' solubilities and the composites' free-volume distributions were then computed. To compute the self-diffusivities of the gases, insertion of the nanotubes was followed by insertion of the gases' molecules into the simulation cell at randomly selected points (without allowing overlaps), followed by energy minimization, compression, and further structural relaxation. In all the cases, ten molecules of each gas were utilized in the diffusion simulations. During all MD simulations, the time step was 1 fs. The temperature was held constant by the Nosé-Hoover method [34], while pressure was fixed by the Andersen method [35]. All softwares used in the simulations have been developed in our group.

B. Force field

All interaction potentials for pure PEI were computed based on the polymer-consistent (PC) force field [36]. The details of the force fields were given previously [13,36], but for completeness are briefly described here. The potential energy associated with bond stretching is given by

$$E_s = \sum_{i=2}^{4} k_i(\ell - \ell_0)^i, \tag{1}$$

where ℓ_0 is the equilibrium length of the bond, ℓ its length during the simulations, and k_i a force constant. The potential energy associated with the deviations of bonds' angles from their equilibrium values is determined by

$$E_\theta = \sum_{i=2}^{4} h_i(\theta - \theta_0)^i, \tag{2}$$

where θ_0 is the equilibrium bond angle, θ its angle during the simulations, and h_i the corresponding force constant. The dihedral (torsional) potential energy of the bonds is given by

$$E_\phi = \sum_{i=2}^{4} d_i(1 - \cos i\phi), \tag{3}$$

with d_i being a force constant and ϕ the dihedral angel. The nonbonded interactions were estimated using a sum of a 6–9 Lennard-Jones (LJ) potential and the standard expression for the Coulombic interactions:

$$E_{nb}(r_{ij}) = \sum_{ij} \epsilon_{ij}\left[2\left(\frac{\sigma_{ij}}{r_{ij}}\right)^9 - 3\left(\frac{\sigma_{ij}}{r_{ij}}\right)^6\right] + \sum_{ij} \frac{q_i q_j}{r_{ij}}, \tag{4}$$

with

$$\sigma_{ij} = \left(\frac{\sigma_i^6 + \sigma_j^6}{2}\right)^{1/6}, \quad \epsilon_{ij} = 2\sqrt{\epsilon_i \epsilon_j}\frac{\sigma_i^3 \sigma_j^3}{\sigma_i^6 + \sigma_j^6}, \tag{5}$$

where σ_i and ϵ_i are the usual LJ size and energy parameters for atom i, r_{ij} is the distance between atoms i and j, and q_i and q_j are their partial electrical charges. In the present study, the potential energy function E_{nb} for the nonbonded interactions was cut off at an interatomic distance of 11 Å. This was based on our previous molecular simulations of the diffusion and sorption of various gases in other nanoporous materials [37,38]. In those studies we used the Ewald summation technique [37] and the multipole expansion method [38,39] in order to account for the Coulombic interactions. Our studies [37,38] indicated that a relatively large cut off distance for computing the contributions of the Coulombic interactions yields reasonably accurate results, while being much simpler than either of the other two methods. Table I lists the force field parameters of CO_2 and CH_4 used in the simulations.

We are not aware of any classical force fields that have been designed for a polymer composite of the type that we are considering in the present paper. If the radius of a SWCNT is large, its properties must be closely related to carbons in graphite, which have sp^2 valence orbital hybridization. Quantum mechanical studies [40] indicate that as the radius decreases, the curvature structure of a nanotube changes valence orbital hybridization and the effective bond order. This leads to hybridization which is close to sp^3, which influences the dynamic fluctuations of the SWCNTs out of their smooth cylindrical structure at zero temperature.

TABLE I. Values of the PC force field for CH_4 and CO_2.

	CH_4			CO_2		
	C	H	C-H	C	O	C-=O
σ (Å)	4.010	2.995		4.010	3.530	
ϵ (kcal/mol)	0.054	0.020		0.064	0.060	
q (electron)	−0.0530	0.01325		0.120	−0.06	
l_0 (Å)			1.101			1.160

Consequently, the potential interaction between gas molecules and the SWCNTs may also be affected. Therefore, it is reasonable to expect that adsorption and diffusion of gas molecules *inside* SWCNTs may also be affected by the change in hybridization. Indeed, this has been found to be the case by Mao *et al.* [16] and others [29,41]. These groups used a variety of classical force fields based on the Brenner potential and its extensions [42]. One may also develop a classical force field for SWCNTs by interpolating between sp^2 and sp^3 values, using the data for sp^2 and sp^3 carbons provided by the self-consistent force field [43].

However, the above results were obtained for diffusion and adsorption *inside* SWCNTs. Our preliminary simulations for the MM PEI structure with SWCNTs indicated that, regardless of the force field used, the gas molecules hardly ever pass *through* the nanotubes. Instead, as described below, the main effect of the nanotubes on the composite polymers is inducing large fluctuations in their accessible free volumes and increasing them, which, in turn, affects diffusion and sorption of gas molecules in the composite polymers. Given that (a) the nanotubes are also composed of carbon atoms and that (b) the PC force field is supposed to be able to represent a variety of polymers and carboneous materials, we used the PC force field to also generate the atomistic models of MM PEI composites. While a more detailed force field would be desirable using, for example, the technique of Ref. [43], we do not believe that such a force field would change the essence of the results that are presented below.

We also point out that the partial charges that are listed in Table I are smaller than those reported previously in the literature and that the carbon van der Waals radius listed in Table I is about 20% larger than what has been reported previously [10–13,44–47]. The reason for the difference is as follows. According to Eqs. (4) and (5), a 6–9 LJ potential, as opposed to the classical 6–12 LJ potential utilized in previous studies, is used in the present work. Moreover, the mixing rules, Eqs. (5), are different from the usual Lorentz-Berthelot rules (arithmetic and geometric averages for the size and energy parameters, respectively) used in most of previous studies. Since the LJ parameters are typically estimated by using experimental data for some properties of a material to fit the parameters of a force field which is used in atomistic simulations, the difference between what is listed in Table I and the previously reported values is natural. This is particularly true if we recall that the parameters of the PC force field represent *optimal values*, designed to reproduce reasonably accurately the morphology of the PEI. As such, they are necessarily not the same as those reported in the literature, even if we had used the 6–9 LJ potential with the Lorentz-Berthelot mixing rules.

C. Estimation of the self-diffusivities

As mentioned above, to estimate the self-diffusivities of CO_2 and CH_4 in the PEI and MM PEI structures, ten molecules of each gas were added to the simulation cell that contains the PEI or MM PEI structure, after which energy minimization, compression, and further relaxation of the system were carried out. The self-diffusivities were then estimated from the mean-square displacements of the gas molecules using the Einstein relation

$$D = \lim_{t\to\infty} \frac{1}{6t}\langle|\mathbf{R}(t) - \mathbf{R}(0)|^2\rangle. \tag{6}$$

Here, $\langle\cdot\rangle$ indicates averages over all gas molecules and over all possible time origins for the motion of the gas molecules and $\mathbf{R}(t)$ is the Cartesian position vector of a gas molecule at time t. The time intervals between the origins were selected to be 100 fs apart.

D. Accessible free volumes and solubilities

To compute the free-volume distributions of the PEI and MM PEI structures, MD simulations in the (*NPT*) ensemble were carried out in the absence of gas molecules. Twenty configurations each of the PEI, MMP7, and MMP12 PEI structures were taken from the simulation trajectories at every 100 fs. The accessible free volumes of the PEI and MM PEI structures were then computed using the following method based on a hard-sphere probe.

(i) The cubic simulation cell was partitioned into a three-dimensional mesh of $100\times100\times100$ subcells.

(ii) A probe molecule (hard sphere) of a given diameter was inserted at the center of each subcell, and the distance to the nearest atom of the material was computed. If the distance turned out to be larger than the sum of the van der Waals radii of the penetrant molecule and the material's atom, the subcell was considered as contributing to the accessible free volume. The cavity size distributions of the PEI and MMP structures were then computed using a Voronoi tessellation of the space based on the algorithm of Tanemura *et al.* [48]. The vectors connecting (the centers of) the atoms in the system were perpendicularly bisected and a large number of intersecting planes were generated. The polyhedra associated with the atoms were then constructed using the al-

gorithm. As a Voronoi polyhedron around an atom identifies its own available space, it can be related to the void volume of the dense amorphous polymer, which was then used to study the evolution of the free volume.

The particle insertion method of Widom [49] was used to estimate the solubility S_0 of the gases in the PEI and MM PEI structures. S_0 is defined as the gas concentration in a volume element of the polymer which is in equilibrium with a given outside reservoir pressure of the same gas. Following the energy minimization, compression, and MD simulation procedure described above, 20 PEI and MM PEI configurations at 20 different times, with intervals of 100 fs in between, were extracted from the MD simulations and used in the simulations with a test particle. The potential parameters for the test particle was also taken from the PC force field. The insertion procedure was then followed by calculating the interaction energy E of the system, consisting of the test particle and the polymers. In the (NPT) ensemble the excess chemical potential μ_e is computed via

$$\mu_e = -k_B T \ln S_0 = -k_B T \ln\langle f_v V \exp(-E/k_B T)/\langle V\rangle\rangle, \quad (7)$$

where T is the temperature, k_B is Boltzmann's constant, f_v is the accessible free-volume fraction, V is the cell's volume during the simulations with $\langle V\rangle$ being its ensemble average, and $\langle\cdots\rangle$ denotes an ensemble average over all the polymers' configurations extracted during the MD simulations. The relation between the solubility S_0 in Eq. (7) and the actual solubility coefficient S in units of cm^3 (STP)/(cm^3 atm) is given by

$$S = \frac{T_0}{T}\frac{1}{P}S_0, \quad (8)$$

with T_0=273.15 K and P_0=1.0 atm.

III. RESULTS

The cell length was about 31 Å for the PEI and 33 and 35 Å for the MMP7 and MMP12 structures, respectively. The density of the materials, after energy minimization, compression, and further relaxation, was about 1.15 g/cm^3 for the MMP7 PEI, 1.1 g/cm^3 for the MMP12 (we are not aware of any data for the densities of the MMP7 and MMP12), and 1.27 g/cm^3 for the PEI structures which is the same as the experimental value. Given the void space that the SWCNTs generate in the MM polymers (see below), their densities appear reasonable, as they are lower than that of PEI.

A typical morphology of the MM polymer in a simulation cell is shown in Fig. 2. To understand the morphology better, we make a rough analogy between the SWCNTs in the PEI structure, on the one hand, and a polymer near a rigid wall, on the other hand (the analogy is not exact, because the nanotubes' walls are not completely rigid and also have curvature). Then, in analogy with the phenomenon of polymer depletion near a rigid wall, one may also expect polymer depletion normal to the long axis of the nanotubes, a phenomenon induced by entropic effects, but also affected by the flexibility of the nanotubes normal to their long axis. Figure 2 indicates this effect.

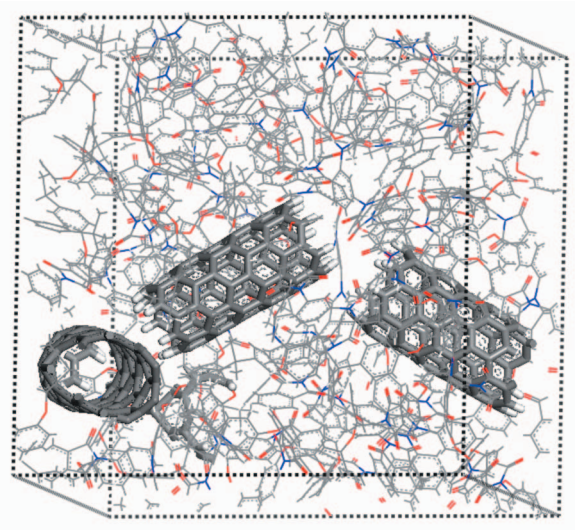

FIG. 2. (Color online) Calculated radial distribution functions of PEI and its composites.

The computed radial distribution functions $g(r)$, defined as the probability of finding atoms at a distance r from another atom compared to the ideal gas distribution, are presented in Fig. 3. The first sharp peak at 1.3 Å is due to the C-H bonding, while the second sharp peak at 1.4 Å is contributed by the C-C bonding in the phenyl rings. Note that, due to the phenyl groups of the nanotubes, the second peaks of the radial distribution functions of the composite polymers are higher than that of PEI. As is well known, the difference between a liquid state and an amorphous polymer is that short-range order in polymers is dominated by the fixed bond lengths associated with the backbone atoms. The radial distribution functions shown in Fig. 3 indicate clearly the amorphous nature of the three polymers—i.e., the complete absence of long-range order.

The time dependence of the free-volume fractions f_v for a probe of size σ=2.5 Å, averaged over 20 configurations taken from the MD simulation in the (NPT) ensemble, is shown in Fig. 4. During the MD simulation in the (NPT) ensemble, fluctuations of f_v were very small. In general, in glassy polymers such as PEI, the characteristic times are so long that the accessible free volumes undergo very small fluctuations. As Fig. 4 indicates, fluctuations of the accessible free volumes in MMP7 and MMP12 are somewhat larger than those in PEI, which is due to the presence of nanotubes and the fluctuations that they induce in the free volume of the polymer chain. These features indicate that the atomistic models that we have generated for PEI and its composites should be quite reasonable.

Figure 5 presents the accessible free-volume fractions f_v, calculated based on a hard-sphere probe and plotted as a function of the probe's diameter (which is represented by its LJ size parameter σ) for PEI and its composites. We took into account the effect of the different densities of PEI and its composites. The values of f_v decrease rapidly with increasing probe diameters. The free-volume fractions are the largest for MMP12, while those of PEI are the smallest. In PEI and MMP7, the accessible free-volume fractions are less

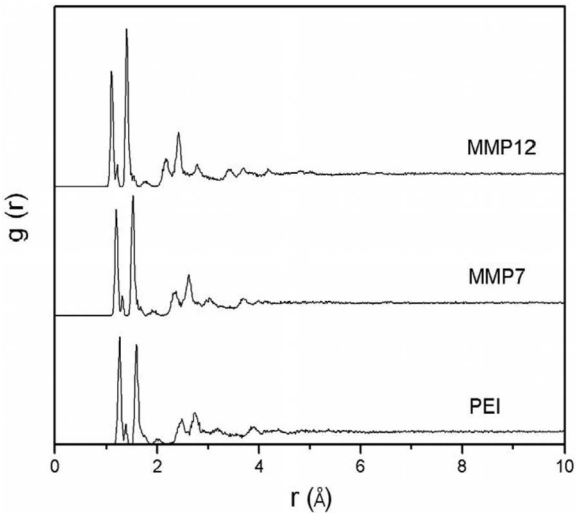

FIG. 3. Fluctuations with the time of the accessible free-volume fractions of PEI and its composites. The probe size is 2.5 Å.

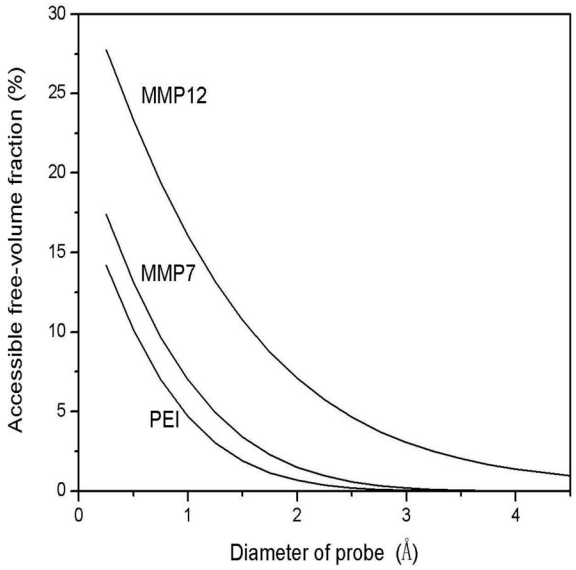

FIG. 5. Three-dimensional view of the mixed-matrix PEI structure within the simulation cell.

than 1% when the probe size is only 3 Å. One might then conclude that the empty volume of the nanotubes contributes significantly to f_v. However, since the difference between values of f_v for PEI and its composites for the smallest probe size is somewhat larger than the empty volumes of the (7,0) and (12,0) nanotubes, we recognize that the increase in f_v in the two polymer composites relative to PEI is, in fact, due to a variety of factors. The most important of such factors is the repulsive interactions between the nanotubes and the polymers' chain, and the fluctuations that such interactions induce in the polymers' morphologies. Figure 5 also indicates that permeation of gas molecules through the polymer composites must be easier than that in PEI, hence already indicating a possible improvement in the separation and transport properties of the composites over pure PEI.

As described earlier, the Voronoi tessellation method was utilized to compute the distributions of the cavity sizes (volumes) for the unit cells of the PEI, MMP7, and MMP12 structures, taking all the atoms into account. The resulting distributions of the cavity sizes (volumes) at three different times are shown in Fig. 6. The shape of the cavity size distribution in the PEI structure is somewhat different from those of its composites, exhibiting distinct "shoulders" that are not seen in the polymer composites. On the other hand, there are small numbers of high-volume cavities in the polymer composites that are not seen in the PEI structure. This is particularly true of MMP12 which has a small, but significant, fraction of cavities with volumes larger than 40 $Å^3$. These features are caused by the absence of the nanotubes in pure PEI and their presence in the polymer composites. The nanotubes squeeze the PEI matrix, hence making the cavity size distributions in the composites more sharply peaked. But they also make it possible to generate a small number of large cavities in the polymer composites, hence opening the way for their improved performance as membranes for gas separation and as composites for other applications. The squeezing effect may be atributed to the repulsive interaction between the polymer and the nanotubes, and is also consistent with the depletion of a polymer near a rigid wall described above. Consistent with Fig. 4, the cavity size distributions do not vary widely with time. Figure 7 presents the ensemble-averaged cavity size distributions at long times.

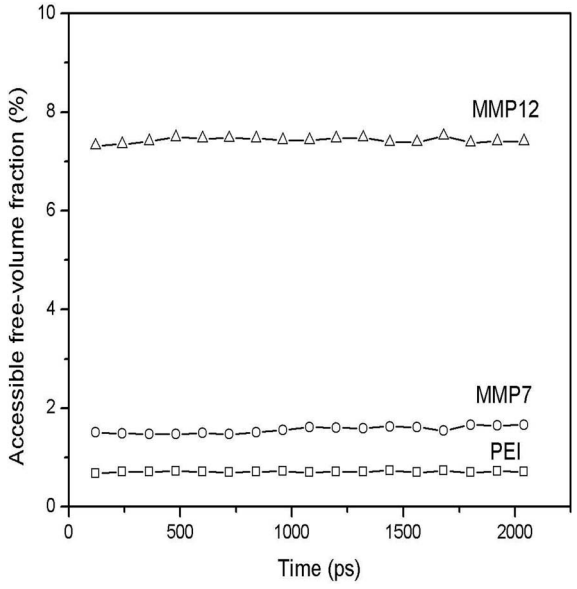

FIG. 4. The distributions of the free-volume fractions of PEI and its composites, averaged over 20 configurations.

As mentioned earlier, the test particle insertion method [49] was used to compute the excess chemical potentials of CH_4 and CO_2 in PEI, MMP7, and MMP12 at 300 K and 1 atm. Figure 8 presents the results. Due to their high free-volume fractions, the excess chemical potentials of the gases in the composite polymers are lower than those in PEI, with the excess chemical potentials in MMP12 being the lowest. In all cases, the excess chemical potentials of CO_2 in the materials are lower than those of CH_4, presumably due to the van der Waals energy and Coulombic charges for

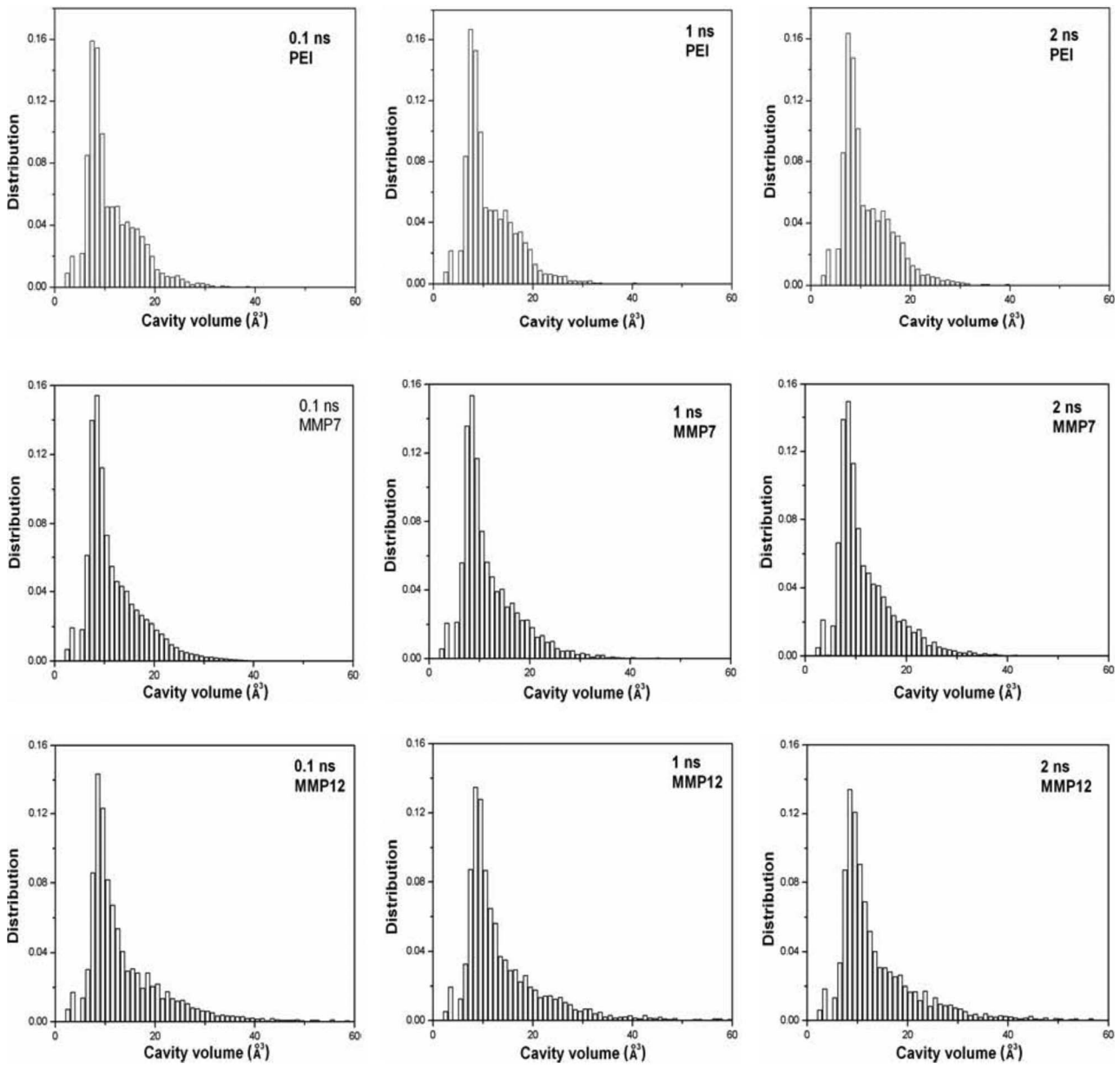

FIG. 6. Time evolution of the cavity volume distributions in PEI and its composites.

CO_2, which are larger than those of CH_4. The fluctuations in the excess chemical potentials are clearly correlated with those of the free-volume fractions shown in Fig. 5.

The computed solubility coefficients are presented in Table II, where, in the case of PEI, they are also compared with the experimental data [50]. In the case of PEI, the computed solubility of CO_2 is about one order of magnitude larger than the measured value, while the computed CH_4 solubility is about a factor of 6 larger the corresponding experimental measurement. The computed ratio is $S_{CO_2}/S_{CH_4} \simeq 8.0$, which should be compred with the measured value of about 3.7. Note that there are some experimental uncertainties in the experimental values of the solubilities, as Henry's law constant, which is derived from fitting experimental sorption isotherm data to the so-called dual-mode sorption model [51], is taken as the experimental value of the solubility. Note also that the difference between the computed and measured solubilities that we are reporting here is about the same as those reported previously [18,19,29].

There are currently no experimental data for MMP7 and MMP12 to compare with our computed values, but as Table II indicates, the polymer composites have much higher gas solubilities than PEI. If we assume that the difference between the computed gases solubilities in MMP7 and MMP12 and the true experimental data (if they were available) are of the same order of magnitude as those for PEI, the results shown in Table II would still indicate gas solubilities in polymer composites that are larger than those in PEI. Since the permeability K of a gas through a membrane is usually defined in terms of its self-diffusivity and solubility, the higher solubilities of the gases in the polymer composites indicate

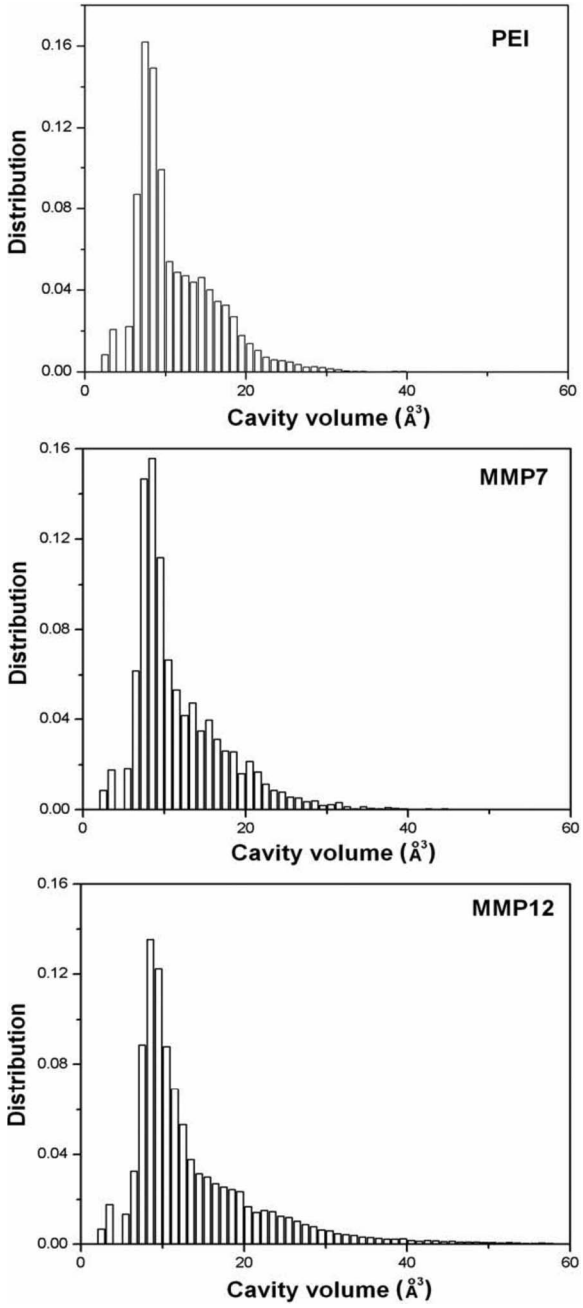

FIG. 7. The distributions of the cavity volumes in PEI and its composites, averaged over 20 realizations.

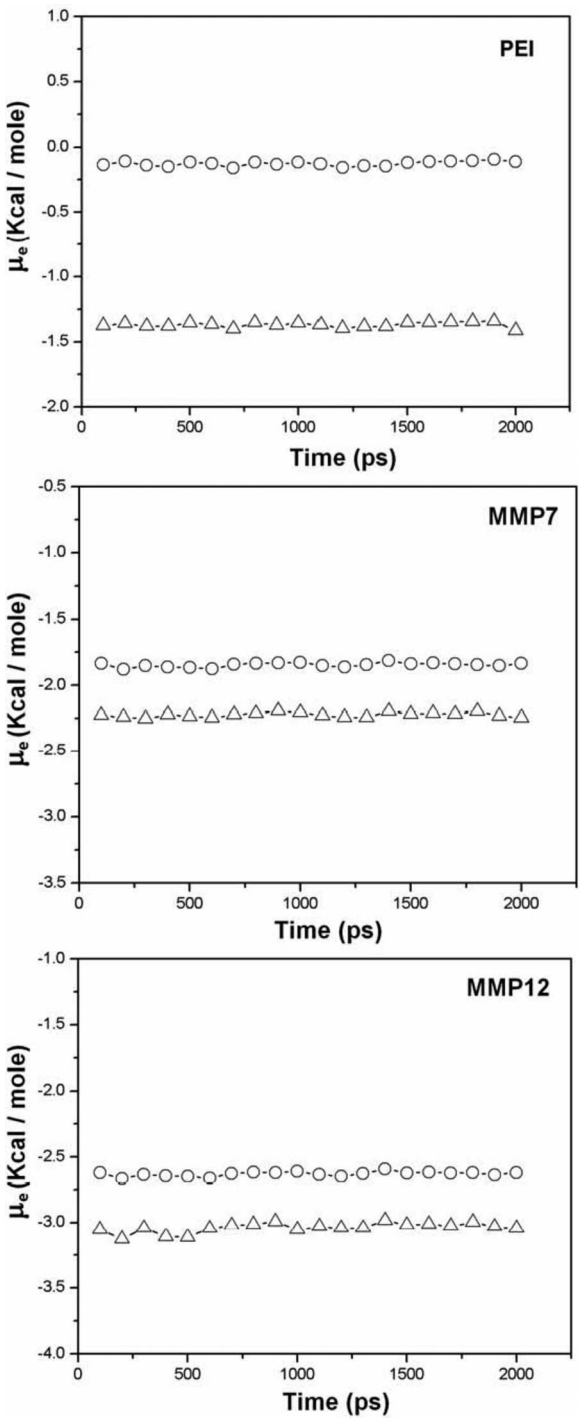

FIG. 8. The excess chemical potentials of CH_4 (circles) and CO_2 (triangles) in the three materials.

that they may also have higher gas permeabilities. We shall return to this point shortly.

We now turn to presenting the results for the self-diffusivities of CO_2 and CH_4. We first note that, in a polymer composite made of one SWCNT and the PEI structure, one would expect the accessible free volume for the diffusion of small gas molecules to be distributed *inhomogeneously* about the long axis of the nanotube. In such a material, the diffusion coefficients may vary *locally*. That is, they will be different if computed for different parts of a polymer composite. The dependence of the diffusivities on the local free-volume fraction may then be described by Doolitles' law

$$D = A \exp\left(-\frac{B}{\eta_{\max} - \eta}\right), \tag{9}$$

or a modification of it [52], where η is the packing fraction of the material with $\eta_{\max}$ being its maximum value, and A and B are constant. In the present work three SWCNTs have been inserted at random into the PEI-structure matrix, which decrease the degree of inhomogeneity about the long axis of any one of them. Therefore, the effective self-diffusivities

TABLE II. Computed and measured solubilities of CH_4 and CO_2.

	PEI		MM7		MM12	
	CO_2	CH_4	CO_2	CH_4	CO_2	CH_4
S (computed)	9.05	1.12	39.05	20.14	149.6	74.95
S (measured)	0.76	0.21				

that we calculate from the slope of the plots of the mean-square displacements (MSDs) versus time should be reasonable indicator of the effect of polymer composites' morphologies on diffusion of small gas molecules through them.

Figures 9 and 10 display, respectively, the ensembles of the gases' trajectories in the simulations cells in the PEI and MMP7 structures, over the length of the simulations. Compared with PEI, the ensemble of the CO_2 trajectories in the MMP7 appears in the form of a large and elongated part of the space which is *around* the nanotubes, rather than a part of the space that include the nanotubes themselves. This is caused by (a) the presence of nanotubes and the squeezing effect that they have on the polymer's morphology (see above) and (b) the depletion phenomenon near the nanotubes. There are also striking differences between the ensembles of the CH_4 trajectories in PEI and MMP7. The enlarged sets of trajectories for both gases also indicate that their effective self-diffusivities in MMP7 (and, hence, MMP12) must be larger than the corresponding values in PEI. As discussed below, this is indeed the case.

To better understand the differences between the trajectories of the two gases in PEI and its composites, we present in Figs. 11 and 12 the time dependence of the displacements $R(t)$ of the two gases in PEI and MMP7, respectively. The fluctuations of $R(t)$ for CO_2 in MMP7 are larger than those in pure PEI by a factor of about 2. Equally striking are the differences between the displacements of CH_4 in PEI and MMP7. While displacements of CH_4 in PEI fluctuate mostly in a narrow band around 3 Å, they vary widely anywhere between 1 and 9 Å in MMP7. The differences are clearly indicative of the restricted morphology of PEI for diffusion of the gases.

These features are all consistent with the hopping mechanism which is often invoked to explain diffusion of small gas

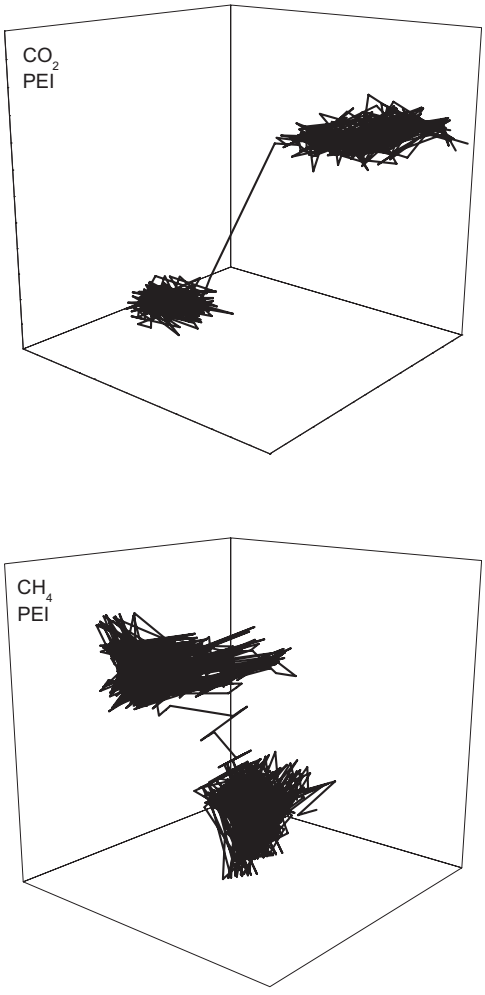

FIG. 9. The ensemble of the trajectories of CO_2 and CH_4 in the PEI structure.

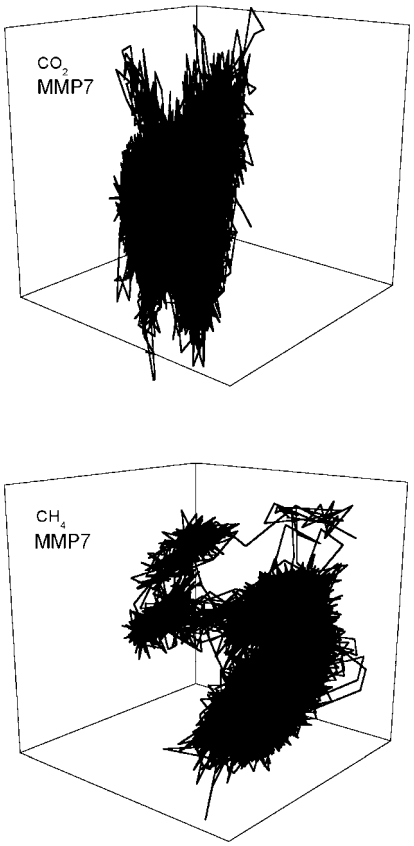

FIG. 10. Same as in Fig. 9, but in the MMP7 structure.

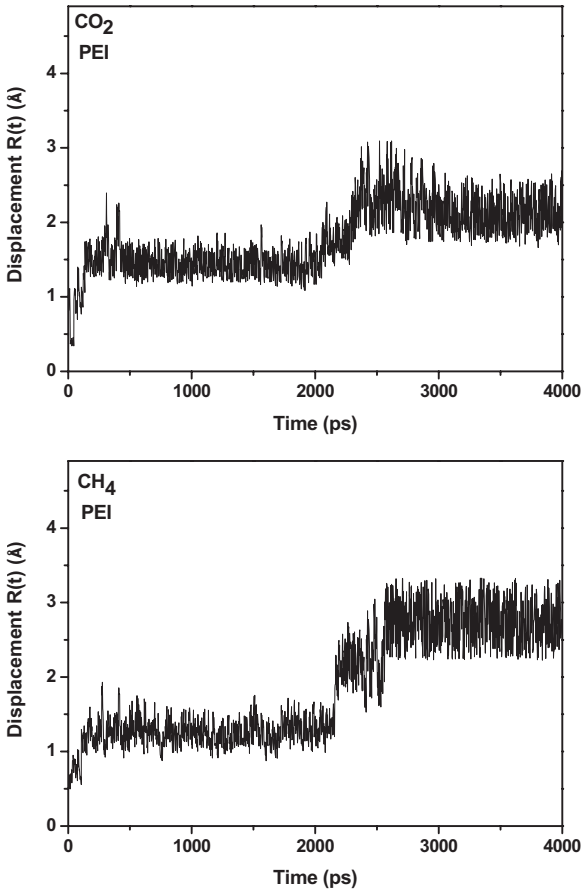

FIG. 11. Time dependence of the displacements of CO_2 and CH_4 from their initial positions in the PEI structure.

molecules in amorphous polymers. According to the hopping mechanism, the gas molecules oscillate in a cavity until the "tunnels" between adjacent cavities are opened, which allows them to hop to the neighboring cavities, provided that they are not already occupied by other gas molecules. The magnitude of the oscillations and the frequency of the hops from one cavity to another depend on the polymer's density and the flexibility of its morphology. In the MD simulations the nanotubes were allowed to be deformable, rather than being rigid structures. Therefore, fluctuations in the deforming nanotubes give rise to increased fluctuations in the PEI chain, hence leading to more frequent hops or jumps of the gas molecules between the cavities. Such fluctuations then explain the larger oscillations and the jump frequencies of the gases in MMP7 (and still larger in MMP12) than those in PEI.

Figures 13 and 14 present the time dependence of the MSDs of the two gases in PEI. In the Fickian regime of diffusion, a plot of log(MSD) versus log(t) must be linear with a slope of 1. Figures 13 and 14 also present such plots, and in both cases the slopes are $\simeq 1$. Moreover, in both cases, the diffusion of the gases reaches the Fickian regime relatively quickly.

The computed self-diffusivities of the two gases in PEI are listed in Table III, along with the experimental data. The computed self-diffusivity of CH_4 is within a factor of 6 of the measured value. As for CO_2, the reported measured self-

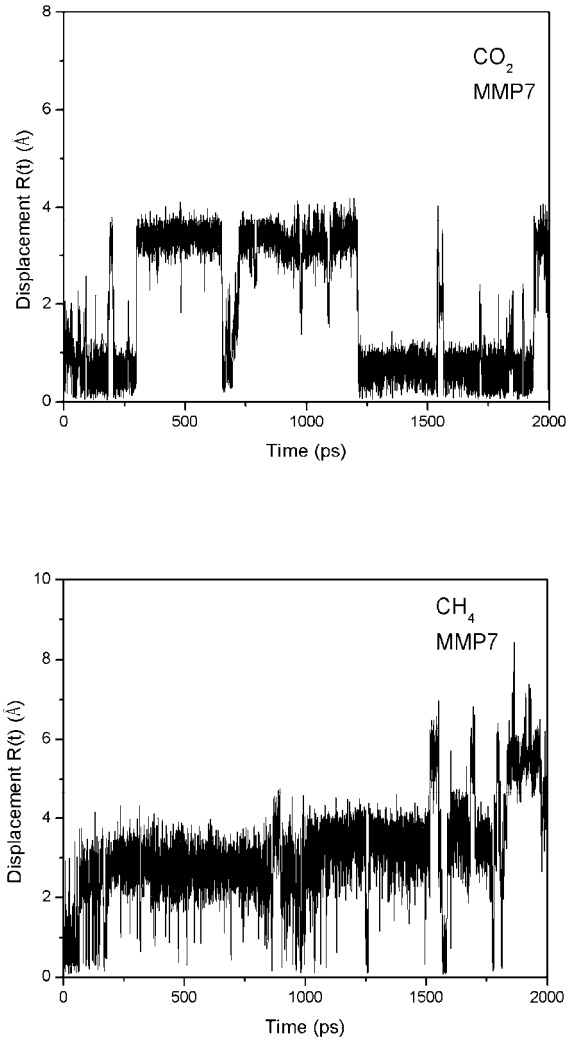

FIG. 12. Same as in Fig. 11, but in the MMP7 structure.

diffusivity of CO_2 in PEI varies by as much as one order of magnitude, ranging (all in cm^2/s) from 11.4×10^{-9} [50] to 7.5×10^{-9} [51] and 1.3×10^{-9} [53]. Therefore, the computed self-diffusivity of CO_2, 5.5×10^{-9} cm^2/s, is just in the middle of the range of the measured values. Given that the parameters of the PC force field have been optimized for accurate representation of the morphology of a class polymers, but not for the transport properties of the gases in them, the agreement between the computed and measured diffusivities of the gases in the PEI is reasonable.

We note one possible qualitative difference between the computed and measured self-diffusivities of the two gases. Whereas the computed self-diffusivities indicate that $D_{CO_2} < D_{CH_4}$, the measured values do not indicate a clear pattern. The two lower measured self-diffusivities reported in the literature [51,53] (see above) are consistent with the pattern of the computed diffusivities, but the highest reported measured self-diffusivity of CO_2 indicates the opposite pattern: namely, that $D_{CO_2} > D_{CH_4}$. This calls for more accurate measurements of the diffusivities in PEI.

As mentioned earlier, we also estimated the self-diffusivities of the two gases in PEI using the (NPT) ensemble. This means that during the MD simulation of the

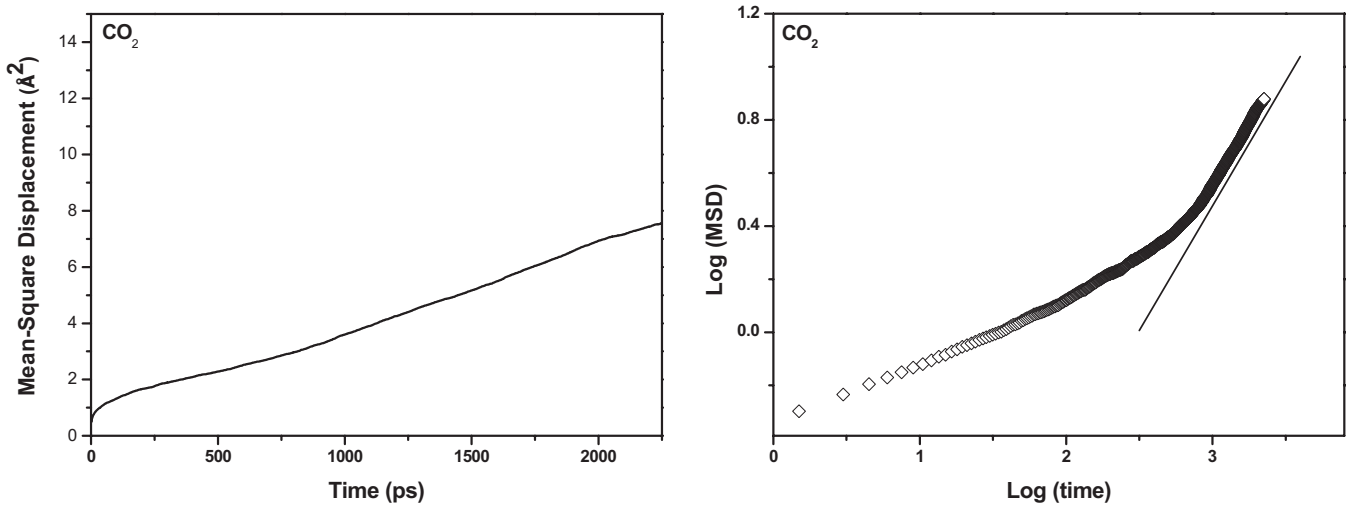

FIG. 13. Time dependence of the MSDs of CO_2 in the PEI structure (left) and its logarithmic plot (right), computed using the (*NPT*) ensemble.

diffusion process the polymer can expand and attain a lower density. Indeed, the density of PEI, which was initially fixed at its experimental value of 1.27 g/cm^3, decreased to, and settled at, 1.19 g/cm^2 after some time, when we carried out the simulations with the (*NPT*) ensemble. Figure 15 presents the resulting MSDs for the two gases obtained with the (*NPT*) ensemble. They result in self-diffusivities that are larger than those reported above, obtained with the (*NVT*) ensemble which holds the volume (and, therefore, the density) of the polymer fixed during the simulations. Such self-diffusivities also indicate that $D_{CO_2} > D_{CH_4}$. One might argue that in an actual experiment in which CO_2 or CH_4 diffuses in a polymer, the volume of the polymer may increase (unless it is somehow prevented from doing so) and, thus, the simulations with the (*NPT*) ensemble might correspond more closely with such an experiment. However, practically all previous MD simulations of the diffusion of gases in various polymers have been carried out in the (*NVT*) ensemble. Moreover, recall that (see above) during the energy minimization and MD simulations of the polymer and the gases' molecules the system is allowed to expand. Thus, we believe that the simulations in the (*NVT*) ensemble are appropriate.

Figure 16 present the time dependence of the MSDs of CO_2 and CH_4 in the two polymer composites, obtained with the (*NVT*) ensemble. The resulting self-diffusivities are also listed in Table III. We are aware of no experimental data for diffusion of the two gases in the two polymer composites. As Table III indicates, the self-diffusivities of both CO_2 and CH_4 in the polymer composites are larger than those in PEI. In particular, the estimated self-diffusivity of CO_2 in MMP12 is larger than in PEI by a factor of more than 2, while that of CH_4 is larger by a factor of about 7. Note that, consistent with the computed self-diffusivities of the two gases in PEI, the ratio D_{CH_4}/D_{CO_2} for the polymer composites is greater than 1. Given the relative accuracy of the gases' effective self-diffusivities in PEI, the results for the polymer composites should also be reasonably accurate.

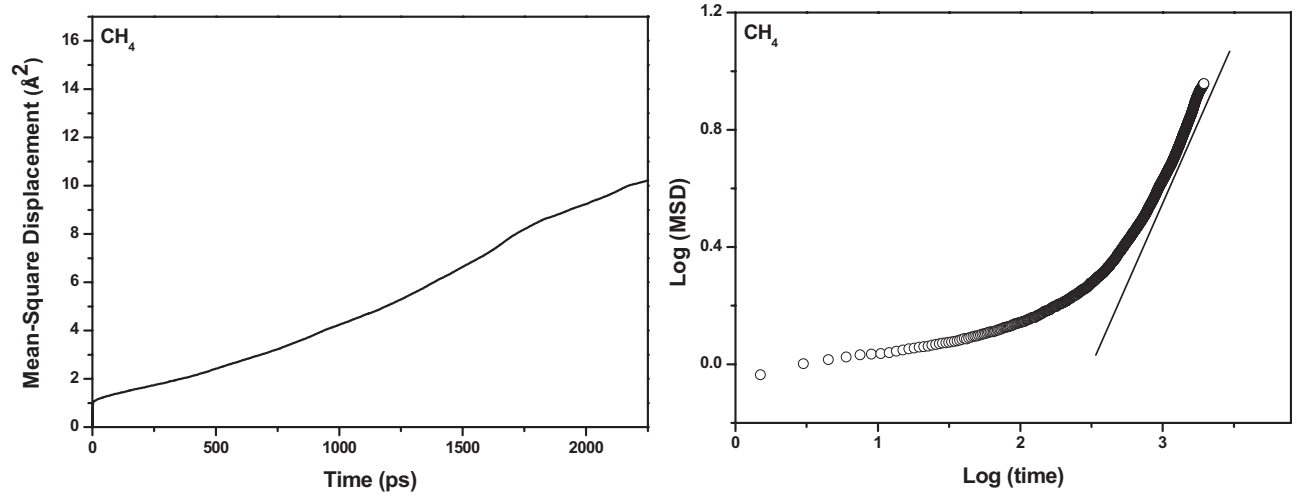

FIG. 14. Same as in Fig. 13, but for CH_4.

TABLE III. Computed and measured self-diffusivities of CH_4 and CO_2, obtained with the (*NVT*) ensemble. All numbers are in cm^2/cs.

	PEI		MM7		MM12	
	CO_2	CH_4	CO_2	CH_4	CO_2	CH_4
$D \times 10^9$ (computed)	5.5	8.0	7.35	16.27	13.73	57.2
$D \times 10^9$ (measured)	1.3–11.4	1.13				

Recall that, as our simulations indicate, the gases' solubilities in the polymer composites, even when we take into account the uncertainties in the computed and measured values, are higher than those in pure PEI (see Fig. 8 and Table II). Then, since the permeability K of a gas through a polymer is defined by

$$K = DS, \tag{10}$$

we may conclude that the polymer composites generated with the carbon nanotubes should have gas permeabilities that are larger than those in PEI by at least a factor of 2–3, when we take into account the uncertainties indicated by Tables II and III. While there are currently no experimental data to compare with our results for polymer composites to confirm our contention, we believe that the results do indicate clearly the possibility of designing MM polymeric membranes, using carbon nanotubes, for gas separation with much improved permeabilities and separation properties than pure polymeric membranes.

It should also be pointed out that in a graphene sheet the conduction and valence bands touch each other at the six corner points of the first Brillouin zone, filled with electrons at the Fermi (highest-)energy level [54,55]. Thus, in general, the sheet behaves as a semimetallic material with a zero band gap. If a nanotube is infinitely long, its electronic states will be parallel lines in the Fourier space. The lines are quantized along the circumference, but continuous along the tube's axis. A (m,n) nanotube can behave as a metallic material if $m=n$, since in this case there are always electronic lines (states) that cross the corner points of the first Brillouin zone. If m-n is *not* a multiple of 3, the electronic states will not pass through the corner points, in which case the nanotube acts as a semiconducting material. But if m-n is a multiple of 3, certain electronic states cross the corner points of the first Brillouin zone, implying that the tube should be semimetallic [55].

Since we have used zigzag $(m,0)$ SWCNTs, the two nanotubes have the two distinct types of electronic properties described above. That is, in the case of the (12,0) nanotube,

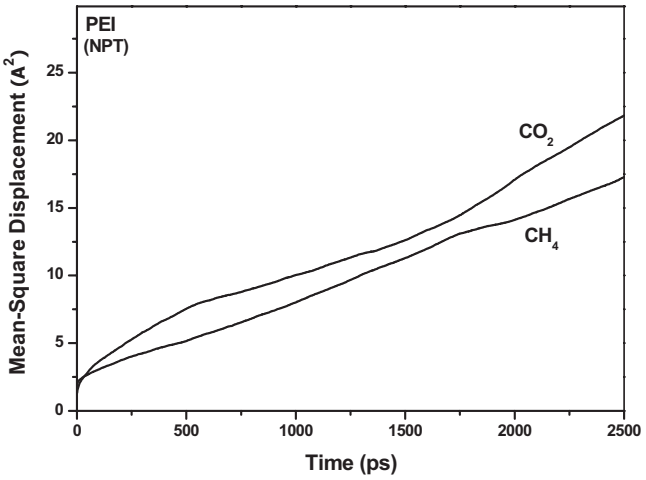

FIG. 15. Time-dependence of the mean-square displacements of CO_2 and CH_4 in the PEI structure, computed using the (*NPT*) ensemble.

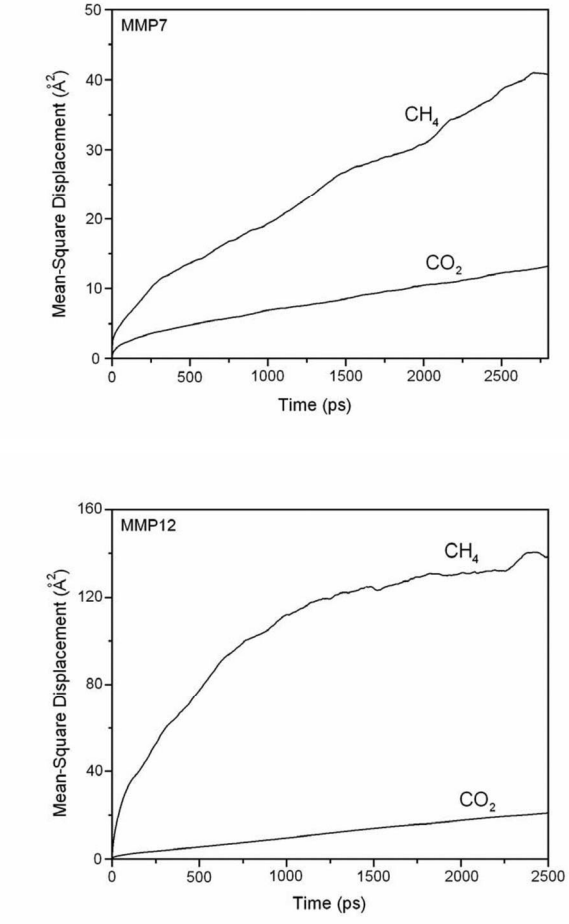

FIG. 16. Time dependence of the MSDs of the two gases in the polymer composites, computing using the (*NVT*) ensemble.

the material is semimetallic, while the (7,0) nanotube should be semiconducting. Thus, it may be that the differences in the diffusion properties of the MM7 and MM12 composites might partly be attributable to the difference between the electronic properties of the two nanotubes. To check this possibility more precisely, one must have a more accurate force field than what we have used in this work. Work in this direction is in progress.

IV. DISCUSSION

In general, one might expect the simple insertion of nanotubes in to a polymer to improve the transport properties of gases through the material, because one might intuitively expect the gas molecules to pass *through* the nanotubes which have smooth potential energy surfaces (provided that their walls are more or less rigid) that give rise to fast transport. However, attributing higher diffusivities to only passages through the nanotubes is naive. The phenomenon is, in fact, far more complex.

First, the nanotubes must have open ends with diameters that are large enough to accomodate the gas molecules. For example, in the present study, the MMP12 material can accomodate both CO_2 and CH_4, as does MMP7 but with somewhat more difficulty.

Second, passage through the nanotube can facilitate transport of the gases through the polymer composite only if either the tubes themselves form percolating paths through the polymer or do so jointly with large cavities (which, however, fluctuate in time). In the present study, we inserted only three SWCNTs in the polymer, hardly enough to form percolating paths for gas transport (see Fig. 2).

Third, if the nanotubes are inserted in the polymer matrix in such a way that the gas molecules can hardly access them (a percolation effect), then no significant improvement in the performance of the MM polymer should be expected, unless the nanotubes can induce creation of larger accessible free volume fraction in the polymer, which is the case here.

The fourth, and perhaps most important, aspect of this phenomenon is that the gas molecules may become essentially trapped in the cavities dispersed in the polymer matrix that originate from entanglement of a polymer chain for periods of time that can be quite long (see Figs. 11 and 12). Therefore, improvement in the performance of the polymer matrix for gas transport depends (in addition to the polymer's density and morphology) on how much the nanotubes can squeeze the polymer matrix to induce fluctuations in its morphology, leading to the creation of large cavities (see above).

It is well known that the transport and solubility of small-size gas molecules are significantly affected by the free-volume distribution in amorphous polymers. It is, of course, of great interest to correlate the free volumes with the self-diffusivities and solubilities. There have been many efforts in the past to determine the free-volume distributions by experimental techniques, such as positron annihilation lifetime spectroscopy (PALS) and photochromic and spin probe methods. In particular, PALS has emerged as a powerful technique, since it provides one with direct and detailed information on the free volume. For example, Hofmann *et al.* [56] compared the results of molecular simulations with the PALS measurements of highly permeable poly(1-(trimethylsilyl)-1-propyne) and moderately permeable polystyrene derivatives, while Nagel *et al.* [57] made the same comparison for polyimide. Dong and Jacob [58] investigated the effect of molecular orientation on the free volume of polyethylene using the Voronoi tessellation technique described above, while Dammert *et al.* [59] studied the relation between the tacticity and free volume of polystyrene by PALS and Voronoi tessellation. It would be of great interest to prepare polymer composites of the type modeled in the present paper and measure the self-diffusivities and solubilities of gases in them in order to confirm the results of the MD simulations reported here.

V. SUMMARY

Atomistic simulations were used to generate models of amorphous polyetherimide and mixed-matrix PEI by inserting carbon nanotubes into a pure polymer. The self-diffusivities of CO_2 and CH_4 in PEI and its mixed-matrix composites at 300 K were estimated using molecular dynamics simulations. In the presence of nanotubes and their repulsive interactions with PEI, there are larger fluctuations in the free-volume distributions of the composites. This is partly reflected in the distributions of the cavity sizes in the PEI, when carbon nanotubes are inserted into it, which take on sharply peaked shapes, but with a few large cavities created in the polymer. As a result, the self-diffusivities of the gases in the mixed-matrix polymers are higher than those in pure PEI.

The solubility coefficients of CO_2 and CH_4 in PEI and its mixed-matrix versions were also computed using molecular simulations. The polymer composites also have higher gas solubilities than PEI, hence indicating that a mixed-matrix polymer that consists of a polymer and carbon nanotubes will have much improved gas permeabilities and separation properties for gaseous mixtures than the original polymer itself.

Clearly, more extensive simulations are needed in order to draw more quantitative conclusions. In particular, one should systematically change the number of nanotubes and also use chiral nanotubes, as opposed to the zigzag ones used in the present study, in order to study their effects. The use of a more accurate force field for representing the nanotubes would also be desirable, as would a study of the diffusion of gases of various sizes in composites. Work on these aspects is in progress.

We note, however, that a recent theoretical study by Hill [60] also indicated that the gases' permeabilities and diffusivities in composite polymeric membranes should be larger than those in a pure polymer. Hill attributed this effect, as we do, to the replusive interactions between the polymer and the

inserted particles. Thus, we believe that the qualitative aspects of our results will remain unchanged, even if more acurate force fields are used. But this assertion remains to be confirmed.

ACKNOWLEDGMENTS

We are grateful to the National Science Foundation, the Department of Energy, and the California Energy Commission for partial support of the work reported in this paper.

[1] *Access in Nanoporous Materials*, edited by T. J. Pinnavaia and M. F. Thorpe (Plenum, New York, 1995).
[2] R. T. Yang, *Gas Separation by Adsorption Processes* (Butterworths, Boston, 1987).
[3] M. Sahimi, Rev. Mod. Phys. **65**, 1393 (1993); *Flow and Transport in Porous Media and Fractured Rock* (VCH, Weinheim, 1995).
[4] J. E. Koresh and A. Sofer, Sep. Sci. Technol. **18**, 723 (1983); C. Bourgerette, A. Oberlin, and M. Inagaki, J. Mater. Res. **7**, 1158 (1992); Y. Hishyama, A. Yoshida, Y. Kaburagi, and M. Inagaki, Carbon **30**, 333 (1992).
[5] C. W. Jones and W. J. Koros, Carbon **32**, 1427 (1994); Ind. Eng. Chem. Res. **34**, 158 (1994); **34**, 164 (1994).
[6] M. B. Shiflett and H. C. Foley, Science **285**, 1902 (1999).
[7] M. G. Sedigh, W. J. Onstat, L. Xu, W. L. Peng, T. T. Tsotsis, and M. Sahimi, J. Phys. Chem. A **102**, 8580 (1998); M. G. Sedigh, L. Xu, T. T. Tsotsis, and M. Sahimi, Ind. Eng. Chem. Res. **38**, 3367 (1999); M. G. Sedigh, M. Jahangiri, P. K. T. Liu, M. Sahimi, and T. T. Tsotsis, AIChE J. **46**, 2245 (2000).
[8] H. Qariouh, R. Schue, F. Schue, and C. Bailly, Polym. Int. **48**, 171 (1999).
[9] M. Sahimi and T. T. Tsotsis, in *Handbook of Theoretical and Computational Nanotechnology*, edited by M. Rieth and W. Schommers (American Scientific, New York, 2006), Chap. 10.
[10] L. D. Gelb, K. E. Gubbins, R. Radhakrishna, and M. Sliwinska-Bartkowiak, Rep. Prog. Phys. **62**, 1573 (1999).
[11] J. Ghassemzadeh, L. Xu, T. T. Tsotsis, and M. Sahimi, J. Phys. Chem. B **104**, 3892 (2000); J. Ghassemzadeh and M. Sahimi, Mol. Phys. **102**, 1447 (2004).
[12] L. Xu, M. Sahimi, and T. T. Tsotsis, Phys. Rev. E **62**, 6942 (2000); L. Xu, T. T. Tsotsis, and M. Sahimi, J. Chem. Phys. **114**, 7196 (2001).
[13] S. Y. Lim, T. T. Tsotsis, and M. Sahimi, J. Chem. Phys. **119**, 496 (2003).
[14] D. Q. Vu, W. J. Koros, and S. J. Miller, J. Membr. Sci. **211**, 311 (2003); **211**, 335 (2003); R. Mahajan and W. J. Koros, Polym. Eng. Sci. **42**, 1420 (2002).
[15] Q. Wang, S. R. Challa, D. S. Sholl, and J. K. Johnson, Phys. Rev. Lett. **82**, 956 (1999); S. R. Challa, D. S. Sholl, and J. K. Johnson, Phys. Rev. B **63**, 245419 (2001); J. Chem. Phys. **116**, 814 (2002).
[16] Z. Mao, A. Garg, and S. B. Sinnott, Nanotechnology **10**, 273 (1999); A. I. Skoulidas, D. M. Ackerman, J. K. Johnson, and D. S. Sholl, Phys. Rev. Lett. **89**, 185901 (2002).
[17] Y. Tamai, H. Tanaka, and K. Nakanishi, Macromolecules **27**, 4498 (1994); **28**, 2544 (1995).
[18] L. Fritz and D. Hofmann, Polymer **38**, 1035 (1997).
[19] F. Muller-Plathe, J. Membr. Sci. **141**, 147 (1998).
[20] S. G. Charati and S. A. Stern, Macromolecules **31**, 5529 (1998).
[21] T. R. Cutherbert, N. J. Wagner, M. E. Paulatis, G. Murgia, and B. D'Auanno, Macromolecules **32**, 5017 (1999).
[22] N. F. A. van der Vergt, W. J. Briels, M. Wessling, and H. Strathmann, J. Chem. Phys. **105**, 8849 (1996).
[23] P. V. Krishna Pant and R. H. Boyd, Macromolecules **26**, 679 (1993); R. K. Bharadwaj and R. H. Boyd, Polymer **40**, 4229 (1999).
[24] R. Zhang and W. L. Mattice, J. Membr. Sci. **108**, 15 (1995).
[25] D. Hofmann, L. Fritz, J. Ulbrich, and D. Paul, Polymer **38**, 6145 (1997); D. Hofmann, L. Fritz, J. Ulbrich, and C. Scherpers, Macromol. Theory Simul. **9**, 293 (2000).
[26] J. R. Fried, M. Sadad-Akhavi, and J. E. Mark, J. Membr. Sci. **149**, 115 (1998); J. R. Fried and D. K. Goyal, J. Polym. Sci., Part B: Polym. Phys. **36**, 519 (1998).
[27] F. Muller-Plathe and W. F. van Gunsteren, J. Chem. Phys. **103**, 4745 (1995); F. Muller-Plathe, H. Liu, and W. F. van Gunsteren, Comput. Theor. Polym. Sci. **139**, 1 (1998).
[28] D. A. Mooney and J. M. D. MacElroy, J. Chem. Phys. **110**, 11087 (1999).
[29] C. Wei, D. Srivastava, and K. Cho, Nano Lett. **2**, 647 (2002).
[30] Y. Han and J. Elliot, Comput. Mater. Sci. **39**, 315 (2007).
[31] E. Tocci, D. Hofmann, D. Paul, N. Russo, and E. Drioli, Polymer **42**, 521 (2001).
[32] M. M. Ostwal, T. T. Tsotsis, and M. Sahimi, J. Chem. Phys. **126**, 124903 (2007).
[33] D. N. Theodorou and U. W. Suter, Macromolecules **18**, 1467 (1985).
[34] S. Nosé, J. Chem. Phys. **81**, 511 (1984); W. G. Hoover, Phys. Rev. A **31**, 1695 (1985).
[35] H. C. Andersen, J. Chem. Phys. **72**, 2384 (1980).
[36] H. Sun, S. J. Mumby, J. R. Maple, and A. T. Hagler, J. Am. Chem. Soc. **116**, 2978 (1994).
[37] N. Kim, Y. Kim, T. T. Tsotsis, and M. Sahimi, J. Chem. Phys. **122**, 214713 (2005); N. Kim, A. Harale, T. T. Tsotsis, and M. Sahimi, *ibid.* (to be published).
[38] A. R. Mehrabi and M. Sahimi, Phys. Rev. Lett. **82**, 735 (1999).
[39] L. Greengard and V. I. Rokhlin, Chem. Scr. **29A**, 139 (1989); H.-Q. Ding, N. Karasawa, and W. A. Goddard III, J. Chem. Phys. **97**, 4309 (1992).
[40] H. Cheng, G. P. Pez, and A. C. Cooper, J. Am. Chem. Soc. **123**, 5845 (2001).
[41] Z. Mao and S. B. Sinnott, J. Phys. Chem. B **104**, 4618 (2000); **105**, 6916 (2001).
[42] D. W. Brenner, Phys. Rev. B **42**, 9458 (1990); J. Che, T. Cagin, and W. A. Goddard III, Theor. Chem. Acc. **102**, 346 (1999).
[43] M. K. Kostov, H. Cheng, A. C. Cooper, and G. P. Pez, Phys. Rev. Lett. **89**, 146105 (2002).
[44] M. J. Hwang, T. P. Stockfisch, and A. T. Hagler, J. Am. Chem. Soc. **116**, 2515 (1994).
[45] W. A. Steele, Langmuir **12**, 145 (1996).

[46] J. Vrabec and J. Fischer, AIChE J. **43**, 212 (1997).
[47] L. Xu, M. G. Sedigh, M. Sahimi, and T. T. Tsotsis, Phys. Rev. Lett. **80**, 3511 (1998); L. Xu, T. T. Tsotsis, and M. Sahimi, J. Chem. Phys. **111**, 3252 (1999); L. Xu, M. G. Sedigh, T. T. Tsotsis, and M. Sahimi, *ibid.* **112**, 910 (2000).
[48] M. Tanemura, T. Ogawa, and N. Ogita, J. Comput. Phys. **51**, 191 (1983).
[49] B. Widom, J. Chem. Phys. **39**, 2808 (1963).
[50] T. A. Barbari, W. J. Koros, and D. R. Paul, J. Polym. Sci., Part B: Polym. Phys. **26**, 709 (1988); **26**, 729 (1988).
[51] H. Kumazawa, J. S. Wang, T. Fukuda, and E. Sada, J. Membr. Sci. **93**, 53 (1994).
[52] J. Budzien, J. D. McCoy, and D. B. Adolf, J. Chem. Phys. **119**, 9269 (2003). One may also consider the Cohen-Turnbull statistical mechanical theory according to which $D=A\exp(-Bv_m/v_f)$, where A and B are constants, v_m is the minimum free volume required for a diffusing molecule to escape its cage of neighboring atoms, and v_f is the available free volume per volume of occupying element; see M. H. Cohen and D. Turnbull, *ibid.* **31**, 1164 (1959).
[53] C. Uriarte, J. Alfageme, and J. J. Iruin, Eur. Polym. J. **34**, 1405 (1998).
[54] M. S. Dresselhaus, G. Dresselhaus, and P. C. Ekland, *Science of Flurenes and Carbon Nanotubes* (Academic Press, San Diego, 1996).
[55] N. Hamada, S.-I. Sawada, and A. Oshiyama, Phys. Rev. Lett. **68**, 1579 (1992); X. Blase, L. X. Benedict, E. L. Shirley, and S. G. Louie, *ibid.* **72**, 1878 (1994).
[56] D. Hofmann, M. Heuchel, Y. Yampolskii, V. Khotimskii, and V. Shantarovich, Macromolecules **35**, 2129 (2002).
[57] C. Nagel, E. Schimidtke, K. Gönther-Schade, D. Hofmann, D. Fritsch, T. Strunskus, and F. Faupel, Macromolecules **33**, 2242 (2000).
[58] H. Dong and K. I. Jacob, Macromolecules **36**, 8881 (2003).
[59] R. M. Dammert, S. L. Maunu, F. H. K. Maurer, I. M. Neelov, S. Nielmelä, F. Sundholm, and C. Wästlund, Macromolecules **32**, 1930 (1999).
[60] R. J. Hill, Phys. Rev. Lett. **96**, 216001 (2006).